Archives of Biochemistry and Biophysics 486 (2009) 141–149

Contents lists available at ScienceDirect

Archives of Biochemistry and Biophysics

journal homepage: www.elsevier.com/locate/yabbi

Structure–function correlation of human programmed cell death 5 protein

Hongwei Yao [a,1], Lanjun Xu [b,1], Yingang Feng [a], Dongsheng Liu [a], Yingyu Chen [b,*], Jinfeng Wang [a,*]

[a] National Laboratory of Biomacromolecules, Institute of Biophysics, Chinese Academy of Sciences, 15 Datun Road, Beijing 100101, China
[b] Laboratory of Medical Immunology, School of Basic Medical Science, Peking University Health Science Center, 38 Xueyuan Road, Beijing 100083, China

ARTICLE INFO

Article history:
Received 4 March 2009
and in revised form 25 March 2009
Available online 7 April 2009

Keywords:
PDCD5
NMR
Structure–function relationship
Cell translocation
Fragments of PDCD5

ABSTRACT

Human programmed cell death 5 (PDCD5) is a translocatory protein playing an important role in the apoptotic process of cells. Although there are accumulated data about PDCD5 function, the correlation of the structure with the function of PDCD5 has not been investigated. Here, we report the studies of structure–function relationship of PDCD5 by multidimensional NMR methods and by FACScan flow cytometer and fluorescence microscope. The 3D structure of intact PDCD5 and the internal motions of PDCD5 have been determined. PDCD5 has a compact core structure of low flexibility with two mobile α-helices at N-terminal region and a flexible unstructured C-terminal region. The flow cytometry and internalization measurements of different PDCD5 fragments indicate that the charged residues are crucial for the ability of apoptosis-promoting and cell translocation of the protein. Combined analyses reveal a fact that the regions that seem to be most involved in the function also are more flexible in PDCD5.

Introduction

Human PDCD5[2] (human programmed cell death 5), formerly designated as TFAR19 (TF-1 cell apoptosis-related gene 19), is a gene cloned from TF-1 cells undergoing apoptosis. PDCD5 protein is an important regulator in both apoptotic and paraptotic cell deaths. The expression of PDCD5 is increased during the apoptotic process of TF-1 cells induced by cytokine withdrawal using a cDNA-RDA method (cDNA representation differences analysis) [1]. The overexpression of PDCD5 can also enhance TAJ/TROY-induced paraptotic cell death, a death pathway distinct from apoptosis [2]. Moreover, the expression of PDCD5 protein is also down-regulated in some human tumors [3–7]. The expressed PDCD5 was found to translocate rapidly from cytoplasm to the cellular nucleus during apoptosis, and the appearance of PDCD5 in the nuclei of apoptotic cells precedes the externalization of phosphatidylserine (PS) and fragmentation of chromosome DNA [8]. The recombinant PDCD5 has a remarkable role in intercellular transport in various cells, serving as a vehicle having potential in the field of protein delivery to the cells. It was observed that PDCD5 can introduce the Mdm-2 binding domain of human p53 into living cells to induce cell death in human cancer cells [9].

PDCD5 containing 125 amino acid residues is a well-conserved protein, sharing significant homology to the corresponding proteins of species ranging from yeast to mice [1]. An orthologue of human PDCD5 in a thermophilic archaeon, MTH1615 (*Methanobacterium thermoautotrophicum* 1615), has 34.2% sequence similarity to the PDCD5 protein (Fig. 1). The 3D solution structure of the protease resistant domain of MTH1615 protein was determined, showing an ordered region which is consisted of three helices (PDB ID: 1EIJ). However, the N-terminal 31 residues of MTH1615 were reported as an unstructured region [10]. For human PDCD5, the early studies have shown that the protein can be divided into three structural regions: a rigid core region and two dissociated terminal regions. The core region (residues 41–101) represents a rigid sub-domain consisting mainly of three α-helices. The C-terminal residues (102–125) represent a flexible unstructured region with a very mobile tail of residues V116-Y125. The N-terminal 38 residues (3–40) are ordered, but not a rigid structural region [11]. A fragment containing the N-terminal 1–26 residues of PDCD5 (PDCD5(1–26)) can form a stable α-helix (D3-A19) in solution (PDB ID: 1YYB) [12]. Recently, the atomic co-ordinates for solution structure of human PDCD5 lacking the N-terminal 1–8 residues (PDCD5(9–113)) appeared in the Protein Data Bank under the accession code 2CRU, which has been determined by RIKEN Structural Genomics/Proteomics Initiative (RSGI). However, there is no report for further studying the relationship of structure and function of PDCD5.

To advance investigations into the structure–function correlation of PDCD5, we have expressed and purified various fragments of PDCD5: PDCD5(1–112), PDCD5(1–104), PDCD5(34–125), PDCD5(34–112), PDCD5(34–104), and PDCD5(20–104) containing

* Corresponding authors. Fax: +86 10 64872026.
E-mail addresses: yingyu_chen@bjmu.edu.cn (Y. Chen), jfw@sun5.ibp.ac.cn (J. Wang).
[1] These authors contributed equally to this work.
[2] *Abbreviations used:* PDCD5, programmed cell death 5; TAJ/TROY, a HGNC (HUGO Gene Nomenclature Committee)-approved symbol TNFRSF19, which is a member of the TNFR (Tumor necrosis factor receptor) superfamily.

0003-9861/$ - see front matter © 2009 Elsevier Inc. All rights reserved.
doi:10.1016/j.abb.2009.03.018

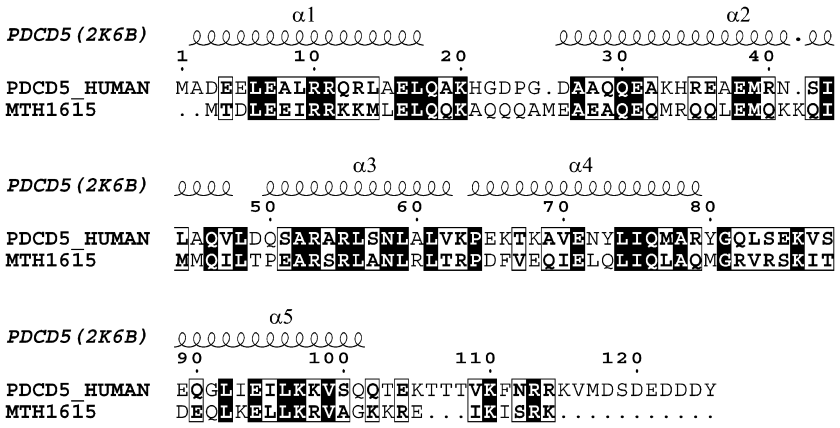

Fig. 1. Sequence alignment of human PDCD5 with MTH1615 from *M. thermoautotrophicus*. The secondary structural elements obtained for PDCD5(1–112) were labeled at the top of the sequences.

residues 1–112, 1–104, 34–125, 34–112, 34–104, and 20–104, respectively. We have employed the fluorescence microscope and FACScan flow cytometer to analyze the functions in the cell translocation and cell apoptosis of different PDCD5 fragments as well as full-length PDCD5. We have determined the solution structure of PDCD5(1–112) and the backbone dynamic features of PDCD5(20–104). The relationship between the structure and the function of PDCD5 was discussed based on the experimental data.

Materials and methods

Preparation of deletion mutants of PDCD5

PDCD5 fragments, namely PDCD5(1–112), PDCD5(1–104), PDC D5(34–125), PDCD5(34–112), and PDCD5(34–104), and PDCD 5(20–104) containing residues 1–112, 1–104, 34–125, 34–112, 34–104, and 20–104, respectively, were used in this study. The fusion expression system used for expression of the intact human PDCD5 was adopted for expression of deletion mutants of PDCD5, except PDCD5(20–104), [13]. The target genes were amplified from the plasmid pET-3d-HR52-PDCD5 and cloned into the pET-3d-HR52 vector with the KpnI and BamHI restriction sites to generate expression plasmids. In each of these expression plasmids, there is a thrombin cleavage site (LVPR↓GS) between the fusion partner HR52, a His_6-tagged N-terminal 52-residue fragment of staphylococcal nuclease R, and the target PDCD5 fragment for removing the fusion partner. For the expression of PDCD5(20–104), the target gene was amplified from the plasmid pET-3d-HR52-PDCD5 and cloned into the NdeI and EcoRI restriction sites of the vector pGBO [14] to generate expression plasmid pGBO-PDCD5(20–104). The expression and purification of PDCD5(20–104) were carried out using similar method as described in the previous study for isolation of PDCD5 protein [11]. As a result of thrombin cleavage, residues Gly-Ser replaced the N-terminal residue M1 in the sequences of PDCD5(1–112) and PDCD5(1–104), and were appended to the N-terminal residue H34 of PDCD5(34–125), PDCD5(34–112), and PDCD5(34–104). Also, four residues Gly-Ser-His-Met are appended to the N-terminal residue K20 of PDCD5(20–104) as a result of the thrombin cleavage.

Uniformly ^{15}N and/or ^{13}C-labeled PDCD5 fragments for NMR studies were obtained by the growth in M9 minimal media containing $^{15}NH_4Cl$ and/or [^{13}C]-glucose as the sole nitrogen and/or carbon sources, respectively. The purity of proteins was checked by SDS–PAGE to ensure a single band.

Preparation of FITC–PDCD5 complex

Fluorescein isothiocyanate (FITC) conjugated recombinant PDCD5 fragment that is FITC–PDCD5 fragment complex was prepared for fluorescence microscopic studies. FITC (Merk) labeling of recombinant PDCD5 fragment was prepared as described previously [15]. Briefly, different recombinant PDCD5 fragments (2 mg/ml) were mixed with DMSO lysed FITC (0.1 mg), and incubated for 16 h at 4 °C. Then, the FITC–PDCD5 fragment complex was further purified using a Sephadex G-50 gel filtration column. The purified FITC–PDCD5 fragment complex was stored in PBS buffer containing 0.1% NaN_3 and 0.1% BSA, and ready for use.

NMR spectroscopy

Samples of uniformly ^{13}C-, ^{15}N-, or $^{13}C/^{15}N$-labelled PDCD5(1–112) for determination of 3D solution structure by NMR method were prepared as follows: 1.0–2.0 mM ^{15}N- or $^{13}C/^{15}N$-labelled PDCD5(1–112) in 90% H_2O/10% D_2O containing 100 mM deuterated acetate buffer (pH 4.7) and 100 mM NaCl; 1.0–2.0 mM ^{13}C-labelled PDCD5(1–112) in 99.996% D_2O containing 100 mM deuterated acetate buffer (pH 4.7) and 100 mM NaCl. The sample for backbone dynamic studies was 1.0 mM ^{15}N-labelled PDCD5(20–104) in 90% H_2O/10% D_2O containing 100 mM deuterated acetate buffer (pH 4.7) and 100 mM NaCl. The sample for hydrogen exchange experiments was 1.0 mM ^{15}N-labelled PDCD5 protein dissolved in 90% H_2O/10% D_2O containing 50 mM phosphate buffer (pH 6.5) and 200 mM NaCl. All the NMR samples contain 0.01% 2,2-dimethyl-2-silapentane-5-sulfonate (DSS) and 0.01% NaN_3.

The heteronuclear NMR experiments were carried out for isotope-labeled PDCD5(1–112) at 308 K on a Bruker DMX600 spectrometer equipped with a z-gradient triple-resonance cryo-probe. The 3D ^1H–^{13}C–^{15}N HNCA, HN(CA)CO, HNCACB, CBCA(CO)NH, H(CC)(CO)NH, and HNCO, 3D ^1H–^{15}N TOCSY-HSQC (τ_m = 60 ms), and 3D ^1H–^{13}C HC(C)H-COSY and HC(C)H-TOCSY (τ_m = 12 ms) experiments [16] were performed for backbone and side chain resonance assignments. The 3D ^1H–^{15}N NOESY-HSQC and ^1H–^{13}C NOESY-HSQC experiments with mixing time τ_m = 200 ms were performed for obtaining the NOE distance constraints. The measurements of ^1H–^{15}N relaxation parameters were performed for ^{15}N-labeled PDCD5(20–104) at 308 K using the standard methods [17]. For ^{15}N T_1 measurements, the delay times were set to 10, 30, 80, 160, 280, 380, 530, 760, 1200, and 1600 ms, whereas for T_2 measurements, the relaxation delays were 16.96, 33.92, 50.88,

67.84, 84.80, 101.76, 118.72, 152.64, 186.56, 220.48, and 254.40 ms. In the 2D ^{1}H–^{15}N NOE experiments, a delay of 3 s was followed by ^{1}H saturation for 6 s, whereas the saturation period was replaced by a delay of equivalent duration in the control experiment. Two experiments were run in an interleaved manner. For amide proton H/D exchange measurements, 2D ^{1}H–^{15}N HSQC spectra of intact PDCD5 were recorded successively after every 245 s at 298 K. Each 2D spectrum required 240 s to complete. All NMR data were processed and analyzed using FELIX98 (Accelrys Inc.). ^{1}H chemical shifts were referenced to internal DSS. ^{15}N and ^{13}C chemical shifts were referenced indirectly [18].

Detecting the cell translocation of PDCD5 fragments

For detecting the structural correlation of internalization of PDCD5, the deletion mutants of PDCD5 were employed. The FITC conjugated PDCD5 fragment complexes: FITC–PDCD5(1–125), FITC–PDCD5(1–112), FITC–PDCD5(1–104), FITC–PDCD5(34–125), FITC–PDCD5(34–112), and FITC–PDCD5(34–104) were constructed. The fluorescence microscopy study was performed by adding these six complexes into cell culture medium.

HL-60 cells were cultured in 35-cm of specialized glass-bottom microwell dishes (MatTek Corp.) with RPMI-1640 medium supplemented with 10% fetal bovine serum (FCS). For fluorescent protein treatments, 1 μM of different FITC–PDCD5 fragment was added. Five-h later, cells were rinsed twice with PBS buffer and fixed with 4% paraformaldehyde in PBS for 15 min at 4 °C. Fixed cells were permeabilized with 0.1% Triton X-100 in PBS for 10 min, washed and stained with DAPI (0.25 μg/ml) for 15 min. Cells were rinsed and imaged using a TCS-SP laser-scanning confocal microscope (Leica Microsystems, Mannheim, Germany).

Detecting the effects of different PDCD5 fragments on cell apoptosis

The promoting-apoptosis effects of intact and different fragments of PDCD5 can be detected by determining the exposure of PS at the surface of apoptotic cells. For this, the apoptotic HL-60 cells were analyzed by flow cytometry using fluorescence-labeled annexin-V [19,20].

HL-60 cells were cultured as described above. For induction of apoptosis, HL-60 cells were washed and adjusted to 2×10^5/ml in serum-free RPMI-1640. Cell suspensions were added into 24-well plates (0.5 ml for each well), and then 20 μg of different recombinant PDCD5 fragment were added. About 20 μg of BSA and etoposide were used as negative and positive controls, respectively. The cells were harvested after treatment for 20 h and washed twice with PBS, followed by resuspending in 100 μl of annexin-V-binding buffer (10 mM Hepes, 140 mM NaCl, 2 mM $MgCl_2$, 5 mM KCl, and 2.5 mM $CaCl_2$, pH 7.4). FITC-conjugated annexin-V (10 μl) (Beijing Biosea Biotechnology Co.) was added according to the manufacturer's protocol. After incubation for 20 min at room temperature in the dark, another 400 μl of binding buffer was added, and samples were immediately analyzed on a FACSCalibur. Cells (1×10^4) were collected and analyzed with CELLQuest software (BD Bioscience). Apoptotic cells are expressed as a percentage of total cells. This experiment was done at least three times.

Structure calculations

Initial structures of PDCD5(1–112) were generated using CANDID module of CYANA software [21]. The NOE assignments given by CANDID were checked manually and the structures were refined in explicit water using CNS software [22] and RECOORDScript [23]. Dihedral angel restrains were obtained using the program TALOS [24]. A family of 100 structures was generated, and the 20 structures with lowest energies were selected for analysis. Structural analysis and statistics were obtained using the programs MOLMOL [25] and PROCHECK-NMR [26]. The molecular figures were generated with MOLMOL.

Analysis of ^{15}N relaxation parameters

R_1 and R_2 relaxation rates for each residue were determined by fitting peak intensities of the spectra acquired at various relaxation delay times to an exponential decay function, $I/I_0 = \exp(-R_{1,2} \cdot t)$, where I_0 is the intensity at $t = 0$ and I is the intensity after a time delay t. The steady-state ^{1}H–^{15}N NOEs were calculated from the ratio of peak intensities in the NOE spectra obtained with and without proton saturation. The uncertainties of the R_1 and R_2 values were estimated from the signal-to-noise ratios. The root-mean-square (RMS) value of the noise of background regions in the spectrum was used to estimate the standard deviation of NOE values.

Results and discussion

3D solution structure of PDCD5(1–112)

As was indicated [11], the C-terminal residues Q102-Y125 of PDCD5 represent a flexible unstructured region. Therefore, 3D structure of PDCD5(1–112) actually is a representative of 3D structure of intact PDCD5. Backbone and side-chain resonance assignments and intramolecular NOE connectivities for PDCD5(1–112) have been identified. More than 99% and 88% backbone and side-chain assignments were achieved, respectively (totally more than 92%). Fig. 2 shows the assignments of amide resonances for

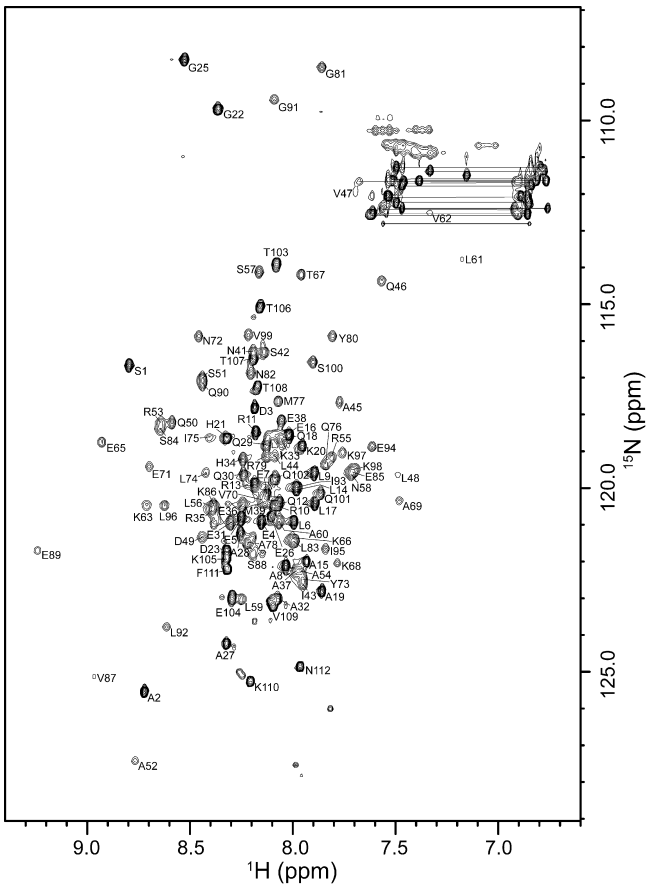

Fig. 2. Residue-specific assignments for backbone amide groups of PDCD5(1–112). The assignments are indicated in the corresponding 2D ^{1}H–^{15}N HSQC spectrum by labeling the one-letter amino acid code and the residue number.

PDCD5(1–112). The number of assigned NOEs is summarized in Table 1. An ensemble of 20 lowest energy NMR-derived solution structures of PDCD5(1–112) is shown in Fig. 3. The structural statistics of the PDCD5(1–112) ensemble are summarized in Table 1.

PDCD5(1–112) is an α-helix protein consisting of five α-helices (α_1:A2-L17, α_2:D26-V47, α_3:Q50-V62, α_4:P64-R79, and α_5:E89-Q101) (Fig. 3A). The helix α_1 shows no NOE connectivity with rest of the PDCD5(1–112) structure, and thus is a dissociated structural region. The helices α_3–α_5 construct a triple-helix bundle, while the helix α_2 connects the helix α_1 and the triple-helix bundle through the loop $L\alpha_1\alpha_2$ (Q18-G25) and the linker $L\alpha_2\alpha_3$ (L48-D49), respectively. The C-terminal fragment (Q102-N112) is an unstructured region (Fig. 3B–D). 16 of 20 hydrophobic residues in the triple-helix bundle: A52, L56, L59, V62, A69, V70, Y73, L74, I75, M77, A78, G91, L92, I95, L96, and V99 form a hydrophobic core together with residues G81, L83, and V87 in the loop $L\alpha_4\alpha_5$ between the helices α_4 and α_5. The side-chains of residues I43, L44, and V47 in the C-terminal region of the helix α_2 and residue L48 in the linker $L\alpha_2\alpha_3$ are also involved in the hydrophobic core (Fig. 4A). The long amphiphilic side-chains of residues R53 and K66 in the helices α_3 and α_4, respectively as well as K63 between the helices α_3 and α_4 can be also placed in the hydrophobic core. Therefore, the segment Q50-Q101 including mainly the triple-helix bundle forms a core structure of the protein.

In the sequence of PDCD5(1–112), there are 37 charged residues. The molecular surface depicting the distribution of electrostatic potential is shown in Fig. 4B. The ionic interactions could be established between some of these charged residues. The tentative salt-bridges were found using distance cutoffs of 4.2 and 6.0 Å. In the loop $L\alpha_4\alpha_5$ (Y80-S88), residues Y80-G81-Q82 construct a β-turn τ1 with residue R79 in the C-terminal of helix α_4 (τ1: R79-Y80-G81-Q82), and residues L83-S88 is close to the structural region around $L\alpha_2\alpha_3$ in the structure of PDCD5(1–112). Thus, residues E85 and K86 in the loop $L\alpha_4\alpha_5$ as well as E89 in the N-terminal end of the helix α_5 form a charged surface with residues D49 in the linker $L\alpha_2\alpha_3$ and R55 in the helix α_3 (Fig. 4C). The pairs of residues R55-E89 and D49-K86 may form two cross-segment salt-bridges on this charged surface, indicating that the N-terminal region of the helix α_3 is close to the N-terminal end of the helix α_5 in the core structure. In addition, residues E71 around the middle of helix α_4 and K98 in the C-terminal region of helix α_5 may also form salt-bridges with residues R40 in the C-terminal region of the helix α_2 and E104 in the C-terminus of PDCD5(1–112), respectively.

Table 1
Restraints and structure statistics for 20 lowest energy conformers of human PDCD5 1–112 fragment.

Parameter	Value
Number of distance restraints	
Total NOEs	2007
Intraresidual NOEs	903
Sequential NOEs	500
Medium range NOEs	407
Long range NOEs	197
Number of dihedral angle restraints	
ϕ angle	82
ψ angle	82
Number of restrain violations (maximum violation)	
Distance restraint violations > 0.2 Å	0 (0.182 Å)
Dihedral angle restrains > 5°	0 (4.28°)
PROCHECK-NMR Ramachandran map analysis (%)	
Most favored regions	87.5
Additional allowed regions	10.4
Generously allowed regions	1.4
Disallowed regions	0.7
RMS deviations (Å) (secondary structure residues)	
α1 helix (residues 2–17)[a]	0.56 ± 0.26; 1.36 ± 0.25[b]
α2 helix (residues 26–47)[c]	1.22 ± 0.57; 1.77 ± 0.50[b]
Core region (residues 41–101)[d]	0.58 ± 0.14; 1.13 ± 0.11[b]
Core secondary structure region(residues 50–62, 64–80, and 89–101)[d]	0.42 ± 0.09; 1.06 ± 0.10[b]

[a] Structures are fitted by backbone heavy atoms of residues 2–17.
[b] For backbone and all heavy atoms, respectively.
[c] Structures are fitted by backbone heavy atoms of residues 26–47.
[d] Structures are fitted by backbone heavy atoms of residues 50–62, 64–80, and 89–101.

Therefore, it appears from the structural information of PDCD5(1–112) that the tertiary interactions including the hydrophobic and cross-segment ionic interactions may play an important role in the packing of the triple-helix bundle in the core structural region. However, there are no indications of the tertiary interactions between residues in the core structure and the residues in the helix α_1, and between the residues in the core structure and the residues in the N-terminal segment (D26-M39) of the helix α_2. For the helix α_2, the C-terminal segment (R40-V47) correlates with the triple-helix bundle by hydrophobic interactions between residues I43, L44, and V47 in the helix, L48 in the loop $L\alpha_2\alpha_3$ and residues L56, L74, I75, A78, L83, and V87 in the triple-helix bundle. Moreover, the ionic interactions between R40 in the helix α_2 and E71 in the helix α_4 may enhance this correlation. Contrary, the N-terminal portion of helix α_2 shows no interactions with the core structure. Such a specific structural construction may account for the unique backbone dynamic features of the helix α_2 as described in the following two chapters.

Dali [27] and SSM [28] searches have provided that the triple-helix bundle structure of human PDCD5 is similar to parts but not entire structure of many proteins. The triple-helix bundle structure of PDCD5(1–112) is very similar to the solution structure of the protease resistant domain of archaeal MTH1615 (SD Fig. 1A in supplementary data) which is 14 residues shorter than human PDCD5 protein (Fig. 1) [10]. The RMSD between human PDCD5(1–112) and archaeal MTH1615 structures aligned by SSM is ~3.05 Å. The significant diversities are observed especially in the N-terminal region. The sequence region representing the helix α_2 according to the structure of PDCD5(1–112) was found to be unstructured in MTH1615. However, the overall structure of PDCD5(1–112) is very similar to PDCD5(9–113) determined by RSGI (SD Fig. 1B).

Different hydrogen-bond-breaking motions of the helices in PDCD5

The structural stability of the intact PDCD5 was probed by H/D exchange which was monitored by a series of 2D ^1H–^{15}N HSQC spectra recorded at 298 K. The 2D ^1H–^{15}N HSQC spectrum of freshly dissolved PDCD5 in D_2O provided cross peaks for 22 amide groups (18% of the 123 residues) (SD Fig. 2). ^1H_N of all other residues in PDCD5 exchanged too rapidly to record in the first spectrum of measurements. Assignments of these 22 resonance signals were straightforward in comparison with the assignments of ^1H_N resonances in the spectrum of PDCD5 [11]. The 22 amide groups are from residues L44 and V47 in the C-terminus of the helix α_2, L48 and D49 in the loop linking the helices α_2 and α_3, R53, R55, and L56 in the helix α_3, V70, E71, Y73-L74-I75-Q76-M77 in the helix α_4, L92-I93-E94-I95-L96-K97 in the helix α_5, V87 in the loop $L\alpha_4\alpha_5$, and the C-terminal residue Y125. Except Y125, these residues reside in the triple-helix bundle of PDCD5, and most of them are involved in the hydrophobic core. Interestingly, these residues are located around the cross-segment ion-pairs D49-K86, R55-E89, E71-R40, and K98-E104. Besides, residues E94-K98 may form a side-chain-to-side-chain lactam bridge in the helix α_5 which can stabilize helix structure [29,30]. After half hour of dissolving PDCD5 in D_2O, only the signals of residues L74, I75, I95, and L96 can be observed in the 2D HSQC spectra. The resonance

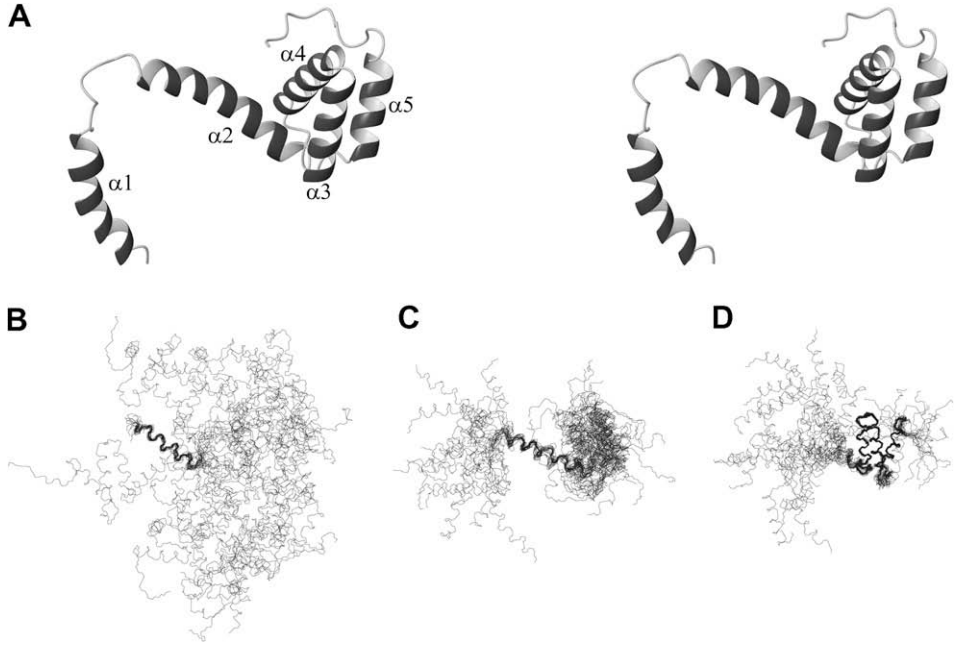

Fig. 3. Solution structure of human PDCD5(1–112). Ribbon structure (A) shows a representative conformer of the ensemble of PDCD5(1–112) structures. The 20 lowest energy conformers calculated for PDCD5(1–112) are superimposed by three different ways: superimposed in the helix α_1 (B), superimposed in the helix α_2 (C), and superimposed in the triple-helix bundle α_3–α_5 (D).

signals for residues I75 and L96 retain their intensities after one hour. These observations reveal that amide protons of residues in the C-terminal unstructured region and the N-terminal helix α_1 of PDCD5 and amide protons of N-terminal residues in the helix α_2 exchanged much faster than those in the helices α_3-α_5. Besides, the residues at the C-terminus of helix α_2 showed much slower H/D exchange than that at the N-terminus.

In D_2O solution, a backbone amide proton of protein exchanges with solvent deuterium, when it is exposed through a transient conformational opening event. The amide protons of residues in the C-terminal unstructured region of PDCD5 are exposed to solvent, thus exchanged with solvent deuterium very fast. In a helix, ^1H_N of *i*th residue and O of $(i-4)$th residue can form a $^1H_{Ni}$–O_{i-4} hydrogen bond. The exchange of the hydrogen-bonded amide protons to the solvent requires occasional opening of the bonds. Amide protons for residues in the helix α_1 and majority residues in the helix α_2 of PDCD5 exchanged too fast to detect their resonance signals in the H/D exchange measurements. This implies that the localized hydrogen-bond-breaking motion (local breathing) of the helix α_1 and the N-terminal portion of the helix α_2 is much faster than the motion of the helices in the triple-helix bundle of the protein. It is quite evident that the triple-helix bundle structure of PDCD5 is stabilized by the tertiary interactions including the hydrophobic and the cross-segment ionic interactions. However, there are no tertiary interactions to stabilize the structure of the helix α_1 and the N-terminal structure of the helix α_2 in PDCD5. The helix α_2 exhibits a relatively stable to very flexible transition in the structure.

Stabilities of different structural regions of PDCD5

The backbone ^1H–^{15}N relaxation parameters, R_1 and R_2 relaxation rates and ^1H–^{15}N NOEs, of intact PDCD5 have been reported early [11]. However, a number of overlapped cross peaks in the 2D ^1H–^{15}N HSQC spectrum of intact PDCD5 prevented us from obtaining more accurate relaxation data for the helix α_2. Obtaining the reliable backbone relaxation data of the helix α_2 is more interesting for analyzing dynamic features of the protein since the helix α_2 connects the N-terminal helix α_1 with the triple-helix bundle of the protein. In this study, the ^1H–^{15}N relaxation parameters were measured for PDCD5(20–104) which lacks 19 and 8 residues in the N- and C-terminal regions, respectively compared to PDCD5(1–112). Deletion of these residues should not disturb the 3D structure of PDCD5(1–112) and the intact PDCD5 as well since both the N- and C-terminal segments have no correlation to the core structure of the protein [11]. Besides, the signal overlapping in the 2D ^1H–^{15}N HSQC spectrum of PDCD5(20–104) is largely reduced. SD Fig. 3 provided spectral evidences that the PDCD5(20–104) is a valid model for investigation of internal motions of the helices α_2–α_5 and the loops linking these helices in PDCD5(1–112).

Fig. 5 shows the relaxation parameters of PDCD5(20–104) at 308 K. In PDCD5(20–104), residues K20-G25 are in the loop $L\alpha_1\alpha_2$ and residues D26-V47 form an ordered helix α_2 while residues Q50-Q101 are in the core structural region of the protein according to the 3D structure of PDCD5(1–112). Sequence variations of the relaxation parameters can be observed for residues K20-M39 in the N-terminus of PDCD5(20–104) including the loop $L\alpha_1\alpha_2$ and the N-terminal portion of the helix α_2, residues Y80-K86 in the loop $L\alpha_4\alpha_5$, and residues S100-E104 in the C-terminus of PDCD5(20–104). These regions are highly flexible with ^1H–^{15}N NOE values < 0.6. The C-terminal residues of the helix α_2 and vast majority residues in the helices α_3, α_4, and α_5 have ^1H–^{15}N NOE values $\geqslant 0.7$, reflecting the relatively restricted high-frequency motions of backbone of the core structural region in PDCD5(20–104). These observations may indicate that the internal motion of the helix α_1 is independent of the rest part of the protein.

Residues forming the helix α_2 (D26-V47) have widely spread R_2 values from 3.68 ± 0.10 to 20.92 ± 0.97 Hz (Fig. 5). In the helix α_2, residues R35-I43 have R_2 values close to those for the residues in the triple-helix bundle. However, residues D26-H34 showed R_2 values decreasing gradually from residue H34 towards D26. Apparently, the internal motions of D26-H34 are less restrictive than residues R35-I43. Thus, a relatively rigid to very flexible transition occurred in the helix α_2. Unexpectedly, residues L44-V47 in the

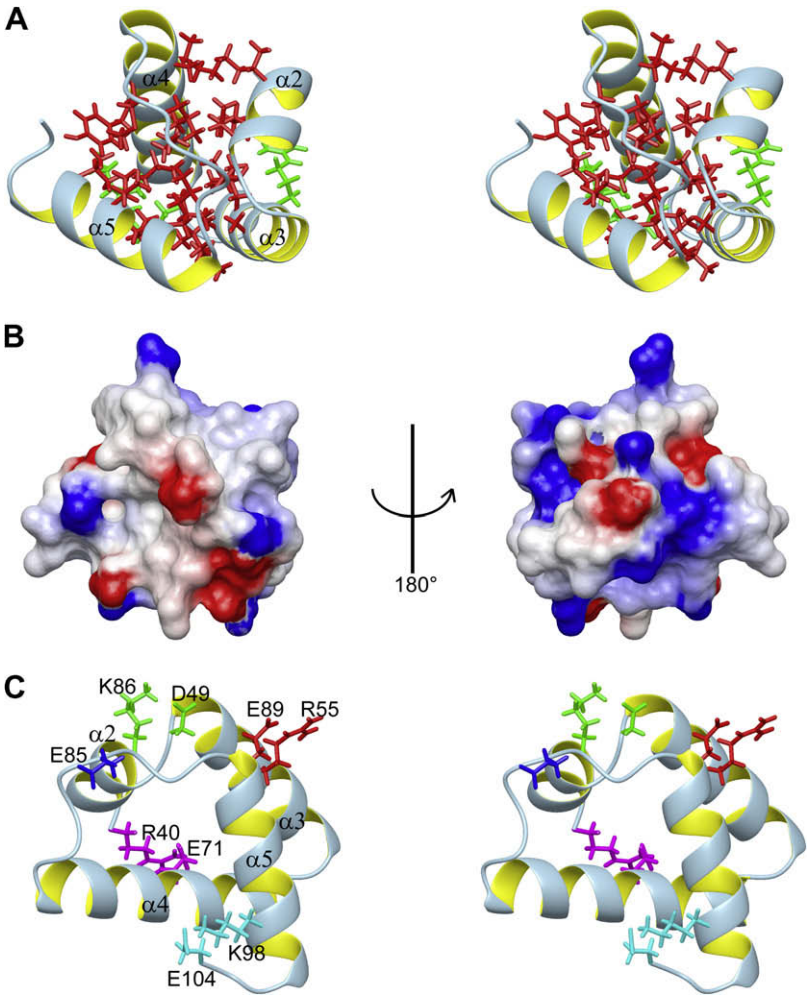

Fig. 4. Analysis of PDCD5(1–112) structure. (A) Hydrophobic core (R40-Q101) of PDCD5(1–112). (B) Molecular surface of the core structure colored by electrostatic potential (blue, positively charged; red, negatively charged; white, neutral). The left-hand representation is the front face and the right-hand one is the back face of potential surface. (C) Charged surface having salt-bridges of the core structure. (For interpretation of the references to color in this figure legend, the reader is referred to the web version of this paper.)

C-terminus of the helix α_2 as well as L48 in the linker $L\alpha_2\alpha_3$ showed significant increase in R_2 but moderately decrease in R_1. Since residues L44-L48 reside in the structural region linking the flexible portion of the helix α_2 and the relatively rigid triple-helix bundle of the protein, the unique dynamic features of these residues probably can be explained if residues L44-L48 are undergoing simultaneously a fast motion and a conformational exchange due to its structural specificity. Therefore, the helix α_2 has a mobile N-terminal portion and a less mobile C-terminal portion which is fixed to the core. The increased R_2 and decreased R_1 values were also observed for residues L61-K63 in the C-terminus of the helix α_3, presumably due to the abrupt transition from one helix to another since the helices α_3 and α_4 run anti-parallel to each other with a turning point at residue K63.

Since the shorter protein PDCD5(20–104) is a valid model in studying the backbone dynamics of the large protein PDCD5(1–112), PDCD5(1–112) can be regarded to have a relatively rigid core structure, and the backbone of this structural region undergoes relatively high restrictive internal motions as compared to the helices α_1 and α_2. The helix α_2 in PDCD5(1–112) has a mobile N-terminal portion and a less mobile C-terminal portion showing relatively restrictive internal motions as the core. Apparently, the unique internal motions of the helix α_2 may be favorable to the helix α_1 for having individual backbone internal motions. In the intact PDCD5, the helix α_1 is mobile and exhibits a slow sub-nanosecond motion as described previously [11].

Evidently, the solution structure of intact PDCD5 consists of a relatively stabilized core structural region, a mobile helix α_1, a partially mobile helix α_2, and an unstructured flexible C-terminal region. Actually, the flexible C-terminal region (Q102-Y125) has a very mobile tail region (V116-MDSDEDDD-Y125) [11]. It was shown that the ^1H–^{15}N NOE and R_2 as well as R_1 values of the segment K105-K115 are higher than the values obtained for tail segment V116-Y125 and lower than the values for segment Q102-E104 in the C-terminal region of PDCD5 [11]. Thus, the segment K105-K115 in intact PDCD5 shows the relatively higher conformational flexibility than the segment Q102-E104 but the reduced backbone flexibility than the tail segment V116-Y125.

Structure–function correlation of PDCD5

The correlation of the internalization with the structure of PDCD5 was demonstrated by the FITC–PDCD5 fragment complexes (SD Fig. 4). The results suggested that both the C-terminal unstructured region and N-terminal helix α_1 of PDCD5 are related with cell translocation, and the C-terminal portion of PDCD5 contains a structural region which is a main region responsible for the cell translocation of the protein.

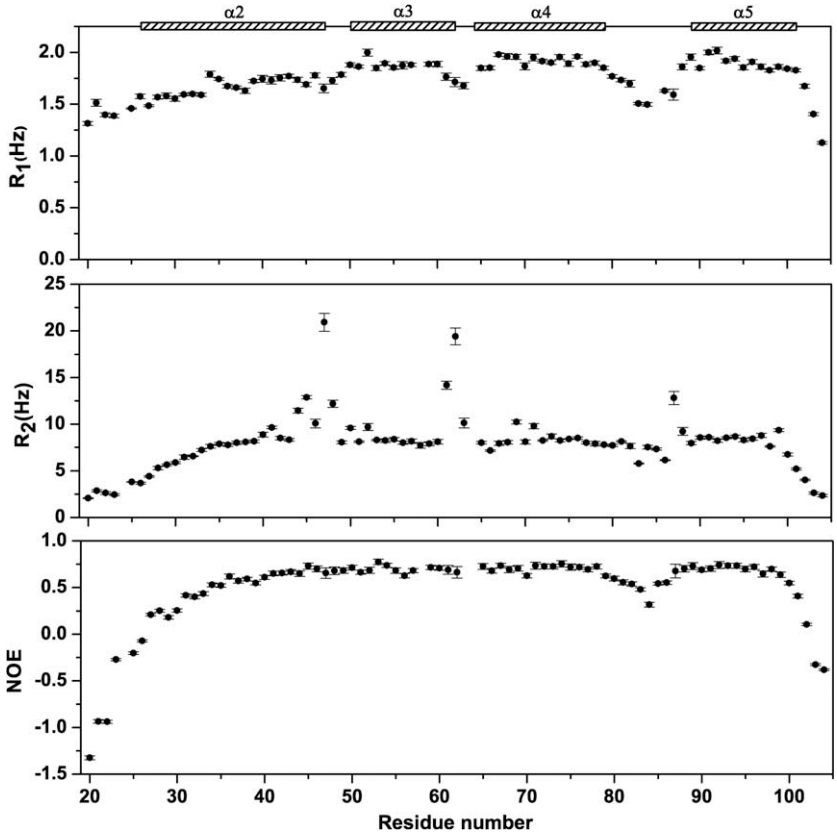

Fig. 5. $^{1}H–^{15}N$ NMR relaxation parameters for PDCD5(20–104). The secondary structures are labeled at the top of the figure.

The effects of different PDCD5 fragments on HL-60 cell apoptosis were observed from the exposure of PS at the surface of apoptotic HL-60 cells determined by flow cytometry using fluorescence-labeled annexin-V [20]. As shown in Fig. 6, PDCD5(1–125) significantly enhanced cell apoptosis induced by serum withdrawal. Deletion of the C-terminal residues R113-Y125 of PDCD5 largely weakened the effect on apoptosis-promoting of FITC–PDCD5(1–112). Further deletion of 8 amino acids in the C-terminal sequence of PDCD5(1–112), namely residues K105-N112, can further weaken (but not much) the effect on apoptosis-promoting of FITC–PDCD5(1–104) compared to those of FITC–PDCD5(1–112). Similar phenomena were observed for PDCD5 lacking the first 33 residues in the N-terminal sequence and having different deletions of the C-terminal residues. Therefore, PDCD5 protein lacking the C-terminal residues can not enhance cell apoptosis triggered by growth factor deprivation. Meanwhile, PDCD5 shortening the N-terminal 33 residues can also influence cell apoptosis. This means the cell apoptosis is correlated with both C-terminal region and N-terminal helix α_1 of PDCD5, but more strongly with the C-terminal region of the protein.

The results of flow cytometry measurements and internalization analysis collectively indicate that there is a close link in PDCD5 between apoptosis-promoting and cell translocation. It appears that the cell translocation and the effect on apoptosis-promoting of PDCD5 are closely related to both terminal regions, especially to the C-terminal region of PDCD5.

According to the M1 value in Fig. 6 which can be considered as a level of HL-60 cell apoptosis, the apoptosis of HL-60 cell treated with intact PDCD5 has the maximum apoptosis level. Truncation of the C-terminal residues R113-Y125 made the fragment PDCD5(1–112) to reduce 14.47% of the apoptosis level as compared to that of intact PDCD5. However, further truncation of the C-terminal residues K105-N112 (fragment PDCD5(1–104)) only reduces additionally 3.88% of the apoptosis level. Therefore, the C-terminal segment R113-Y125 might be more responsible for the cell apoptosis than the segment K105-N112. The segment R113-Y125 contains not only positive charged residues R113, R114, and K115 but also negative charged residues D118-X-D-E-D-D-D124 and aromatic residue Y125. The segment K105-N112 contains two basic residues K105 and K110 and one aromatic residue F111. It was also reported that EGFP–PDCD5(1–115) was internalized while EGFP–PDCD5(1–108) was almost not internalized when HEK293 cells were incubated with EGFP–PDCD5 fusion protein, suggesting that residues V109-K115 might be important for the capability of PDCD5 to translocate through plasma membranes [9].

The recent research has suggested that PDCD5 behaves as a molecule similar to Tat involved in lipid rafts/caveolae endocytosis, making use of clathrin-independent endocytosis to enter the cells [9]. The Tat-PTD, a protein transduction domain consisting of GRKKRRQRRRPPQ, can be used to transport oligonucleotides, peptides, and proteins into a broad range of cell types [31]. The lipid rafts or caveolae is referred to the membrane domain containing sphingolipids and cholesterol. The sphingolipids include glycosphingolipids (GSL) and sphingomyelin (SM). Here, GSL may be either neutral or negatively charged in the case of ganglioside, a sialic acid-containing cell surface GSL. SM carries one positive and one negative charge. The interactions of protein with lipid rafts may be achieved through electrostatic interactions between the charged residues (preferentially basic) of protein and the polar heads of SM and gangliosides. Furthermore, a conveniently oriented solvent-exposed aromatic side-chain can stack on the sugar ring of GSL [32].

Based on the above experimental information, it can be considered that residues K105-K115 in the C-terminal region of PDCD5

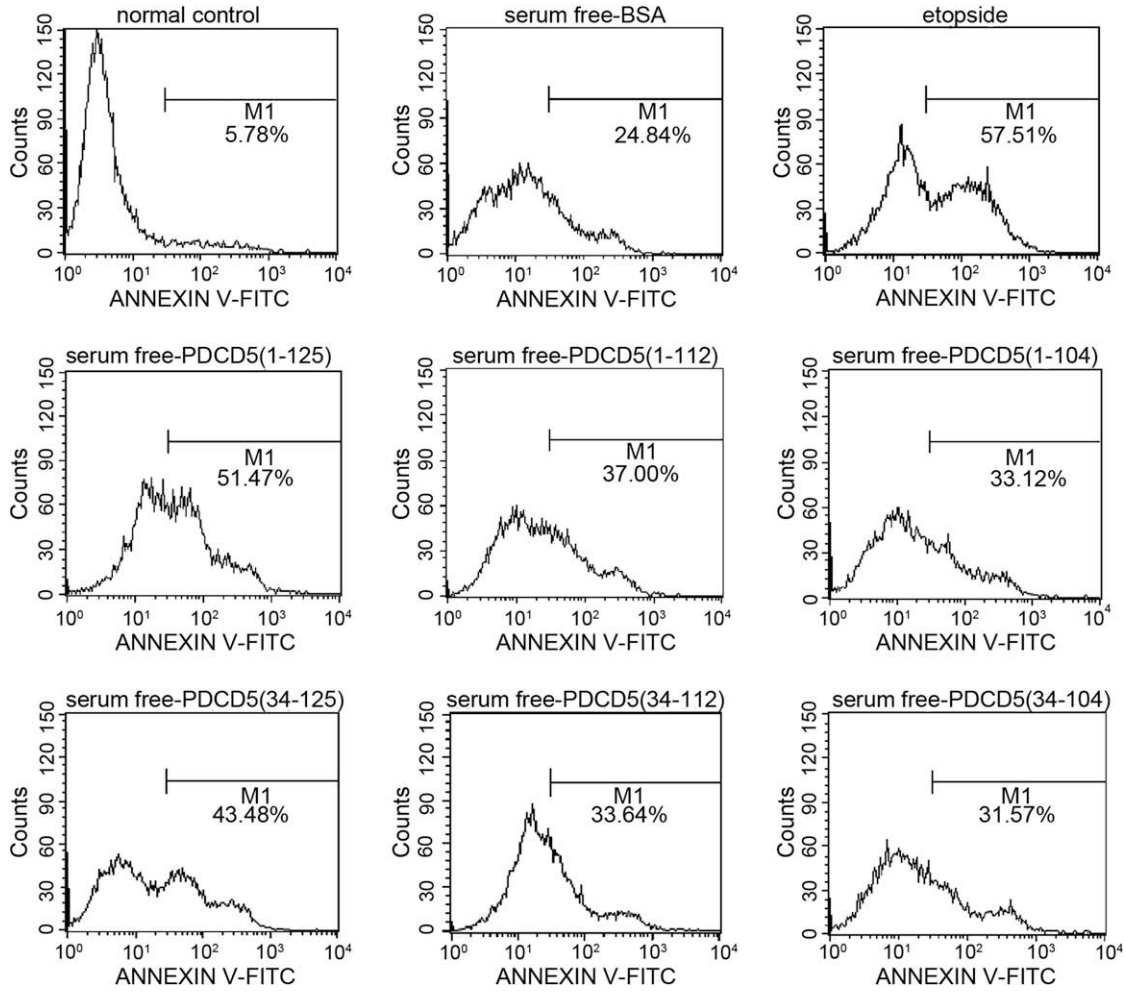

Fig. 6. Flow cytometric analysis of HL-60 cell apoptosis induced by serum withdrawal. HL-60 cells were treated with the different PDCD5 fragments at concentration of 20 μg/ml. Percentages of cell apoptosis were determined by flow cytometry with annexin-V–FITC. Numbers of M1 indicate the corresponding proportions of apoptotic cells that display positive annexin-V–FITC labelling. BSA and etoposide were used as negative and positive controls, respectively. Experiments were performed at least in triplicate, with similar results.

might be more crucial for the biological function of the protein since it contains 5 basic amino acids K105, K110, R113, R114 and K115 and one aromatic amino acid F111. Besides, the dynamic features of segment K105-K115 may facilitate the interactions of the basic and aromatic residues with the polar heads of SM and gangliosides in lipid rafts of the plasma membrane. On the other hand, residues D118-SDEDDD-Y125 in the tail of PDCD5 probably can interact with the positive charges of SM and the sugar ring of GSL in the lipid rafts of cell membrane, since the mobile tail is very flexible in conformation. Presumably, the biological function of PDCD5 has close relation to the distribution of charged residues and the conformational flexibility of corresponding sequence regions in the protein, since the apoptosis-promoting is closely linked to the cell translocation.

Fragment PDCD5(34–125) was obtained by deletion of N-terminal 33 residues: MADEELEALRRQRLAELQAKHGDPGDAAQQEAK which constructs the helix α_1 (A2-L17) and the loop L$\alpha_1\alpha_2$ as well as the N-terminal residues (D26-K33) of the helix α_2. Similar to the C-terminal of PDCD5, the N-terminal helix α_1 is more flexible than the main part of the protein and provides the negative and positive charged residues DEE-E-RR-R. These charged residues may also interact with lipid rafts, which can account for the observed phenomena in the cell translocation and the apoptosis-promoting effect of PDCD5 caused by deletion of the helix α_1.

The above analysis reveals a fact that the regions that seem to be most involved in the function also are more flexible in PDCD5. Whether this could be pure coincidence remains a question. However, a conjecture can be made from this fact that the charged residues of PDCD5 are crucial for the ability of apoptosis-promoting and cell translocation of PDCD5, and the location of the charged residues in the conformational flexible regions may be also a positive factor for PDCD5 to exert its biological functions.

Accession numbers

The atomic coordinates and NMR restraints of PDCD5(1–112) have been deposited in the Protein Data Bank under ID code 2K6B. The chemical shifts of ^{1}H, ^{15}N, and ^{13}C resonances for PDCD5(1–112) have been deposited in the BioMagResBank database with accession number 15864.

Acknowledgments

J.W. was supported by the National Natural Science Foundation of China (NNSFC 30170201), the 863 Special Program of China (Grant No. 2002BA711A13) and the Key Important Project from Chinese Academy of Sciences (Grant No. KSCX1-SW-17).

Appendix A. Supplementary data

Supplementary data associated with this article can be found, in the online version, at doi:10.1016/j.abb.2009.03.018.

References

[1] H. Liu, Y. Wang, Y. Zhang, Q. Song, C. Di, G. Chen, J. Tang, D. Ma, Biochem. Biophys. Res. Commun. 254 (1999) 203–210.
[2] Y. Wang, X. Li, L. Wang, P. Ding, Y. Zhang, W. Han, D. Ma, J. Cell Sci. 117 (2004) 1525–1532.
[3] I. Hedenfalk, D. Duggan, Y. Chen, M. Radmacher, M. Bittner, R. Simon, P. Meltzer, B. Gusterson, M. Esteller, O.P. Kallioniemi, B. Wilfond, A. Borg, J. Trent, M. Raffeld, Z. Yakhini, A. Ben-Dor, E. Dougherty, J. Kononen, L. Bubendorf, W. Fehrle, S. Pittaluga, S. Gruvberger, N. Loman, O. Johannsson, H. Olsson, G. Sauter, N. Engl. J. Med. 344 (2001) 539–548.
[4] X.R. Xu, J. Huang, Z.G. Xu, B.Z. Qian, Z.D. Zhu, Q. Yan, T. Cai, X. Zhang, H.S. Xiao, J. Qu, F. Liu, Q.H. Huang, Z.H. Cheng, N.G. Li, J.J. Du, W. Hu, K.T. Shen, G. Lu, G. Fu, M. Zhong, S.H. Xu, W.Y. Gu, W. Huang, X.T. Zhao, G.X. Hu, J.R. Gu, Z. Chen, Z.G. Han, Proc. Natl. Acad. Sci. USA 98 (2001) 15089–15094.
[5] X. Ma, G. Ruan, Y. Wang, Q. Li, P. Zhu, Y.Z. Qin, J.L. Li, Y.R. Liu, D. Ma, H. Zhao, Clin. Cancer Res. 11 (2005) 8592–8599.
[6] M. Spinola, P. Meyer, S. Kammerer, F.S. Falvella, M.B. Boettger, C.R. Hoyal, C. Pignatiello, R. Fischer, R.B. Roth, U. Pastorino, K. Haeussinger, M.R. Nelson, R. Dierkesmann, T.A. Dragani, A. Braun, J. Clin. Oncol. 24 (2006) 1672–1678.
[7] Y.H. Yang, M. Zhao, W.M. Li, Y.Y. Lu, Y.Y. Chen, B. Kang, Apoptosis 11 (2006) 993–1001.
[8] Y. Chen, R. Sun, W. Han, Y. Zhang, Q. Song, C. Di, D. Ma, FEBS Lett. 509 (2001) 191–196.
[9] Y. Wang, D. Li, H. Fan, L. Tian, Y. Zhong, Y. Zhang, L. Yuan, C. Jin, C. Yin, D. Ma, J. Biol. Chem. 281 (2006) 24803–24817.
[10] D. Christendat, A. Yee, A. Dharamsi, Y. Kluger, A. Savchenko, J.R. Cort, V. Booth, C.D. Mackereth, V. Saridakis, I. Ekiel, G. Kozlov, K.L. Maxwell, N. Wu, L.P. McIntosh, K. Gehring, M.A. Kennedy, A.R. Davidson, E.F. Pai, M. Gerstein, A.M. Edwards, C.H. Arrowsmith, Nat. Struct. Biol. 7 (2000) 903–909.
[11] D. Liu, Y. Feng, Y. Cheng, J. Wang, Biochem. Biophys. Res. Commun. 318 (2004) 391–396.
[12] D. Liu, H. Yao, Y. Chen, Y. Feng, J. Wang, Biochem. J. 392 (2005) 47–54.
[13] Y.M. Feng, Y.M. Zhang, G.Z. Jing, Protein Expr. Purif. 25 (2002) 323–329.
[14] Y. Cheng, D.J. Patel, Biochem. Biophys. Res. Commun. 317 (2004) 401–405.
[15] R.F. Masseyeff, W.H. Albert, N.A. Staines, Methods of Immunological Analysis, John Wiley & Sons, 1993, pp. 237–238.
[16] J. Cavanagh, W.J. Fairbrother, A.G. Palmer, N.J. Skelton, Protein NMR Spectroscopy: Principles and Practice, Academic Press, San Diego, 1996.
[17] N.A. Farrow, R. Muhandiram, A.U. Singer, S.M. Pascal, C.M. Kay, G. Gish, S.E. Shoelson, T. Pawson, J.D. Forman-Kay, L.E. Kay, Biochemistry 33 (1994) 5984–6003.
[18] J.L. Markley, A. Bax, Y. Arata, C.W. Hilbers, R. Kaptein, B.D. Sykes, P.E. Wright, K. Wuthrich, Pure Appl. Chem. 70 (1998) 117–142.
[19] V.A. Fadok, D.L. Bratton, S.C. Frasch, M.L. Warner, P.M. Henson, Cell Death Differ. 5 (1998) 551–562.
[20] J.D. Smith, C. Waelde, A. Horwitz, P. Zheng, J. Biol. Chem. 277 (2002) 17797–17803.
[21] T. Herrmann, P. Guntert, K. Wuthrich, J. Mol. Biol. 319 (2002) 209–227.
[22] A.T. Brunger, P.D. Adams, G.M. Clore, W.L. DeLano, P. Gros, R.W. Grosse-Kunstleve, J.S. Jiang, J. Kuszewski, M. Nilges, N.S. Pannu, R.J. Read, L.M. Rice, T. Simonson, G.L. Warren, Acta Crystallogr. D. Biol. Crystallogr. 54 (1998) 905–921.
[23] A.J. Nederveen, J.F. Doreleijers, W. Vranken, Z. Miller, C.A. Spronk, S.B. Nabuurs, P. Guntert, M. Livny, J.L. Markley, M. Nilges, E.L. Ulrich, R. Kaptein, A.M. Bonvin, Proteins 59 (2005) 662–672.
[24] G. Cornilescu, F. Delaglio, A. Bax, J. Biomol. NMR 13 (1999) 289–302.
[25] R. Koradi, M. Billeter, K. Wuthrich, J. Mol. Graph. 14 (1996) 51–55.
[26] R.A. Laskowski, J.A. Rullmannn, M.W. MacArthur, R. Kaptein, J.M. Thornton, J. Biomol. NMR 8 (1996) 477–486.
[27] L. Holm, C. Sander, J. Mol. Biol. 233 (1993) 123–138.
[28] E. Krissinel, K. Henrick, Acta Crystallogr. D. Biol. Crystallogr. 60 (2004) 2256–2268.
[29] M.E. Houston Jr., A.P. Campbell, B. Lix, C.M. Kay, B.D. Sykes, R.S. Hodges, Biochemistry 35 (1996) 10041–10050.
[30] D.F. Mierke, S. Maretto, E. Schievano, D. DeLuca, A. Bisello, S. Mammi, M. Rosenblatt, E. Peggion, M. Chorev, Biochemistry 36 (1997) 10372–10383.
[31] S.R. Dennison, R.D. Baker, I.D. Nicholl, D.A. Phoenix, Biochem. Biophys. Res. Commun. 363 (2007) 178–182.
[32] N. Taieb, N. Yahi, J. Fantini, Adv. Drug Deliv. Rev. 56 (2004) 779–794.